Interannual variability of Caribbean rainfall, ENSO and the Atlantic Ocean

Alessandra Giannini, Yochanan Kushnir and Mark A. Cane

Lamont-Doherty Earth Obs. of Columbia University

Palisades, NY 10964

J. Climate 13:297-311, 2000

Copyright by the American Meteorological Society

Contribution 5919 of Lamont-Doherty Earth Observatory

Abstract

The large-scale ocean-atmosphere patterns that influence the interannual variability of Caribbean-Central American rainfall are examined. The atmospheric circulation over this region is shaped by the competition between the north Atlantic subtropical high sea level pressure system and the eastern Pacific intertropical convergence zone (ITCZ), which influence the convergence patterns on seasonal and interannual timescales.

We find the leading modes of interannual sea level pressure (SLP) and sea surface temperature (SST) variability associated with Caribbean rainfall, as selected by canonical correlation analysis, to be an inter-basin mode, linking the eastern Pacific with the tropical Atlantic, and an Atlantic mode. North Atlantic SLP affects Caribbean rainfall directly, by changing the patterns of surface flow over the region, and indirectly, through SST anomalies. Anomalously high SLP in the region of the North Atlantic high translates into stronger trade winds, hence cooler SSTs, and less Caribbean rainfall. The inter-basin mode, which manifests itself as a zonal seesaw in SLP between the tropical Atlantic and the eastern equatorial Pacific, is correlated with ENSO. When SLP is low in the eastern equatorial Pacific, it is high in the tropical Atlantic: the surface atmospheric flow over the basin is divergent, to the west, toward the eastern Pacific ITCZ, and to the east, toward the tropical North Atlantic. A weakened meridional SLP gradient in the tropical North Atlantic signifies weaker trade winds and the opportunity for SSTs to warm up, reaching peak intensity two to four months after the mature phase of an ENSO event. This SST anomaly is particularly evident in the Caribbean-western Atlantic basin.

The tendency is for drier-than-average conditions when the divergent atmospheric flow dominates, during the rainy season preceding the mature phase of a warm ENSO event. The dry season that coincides with the mature phase of ENSO is wetter than average over the northwestern section of the basin, i.e. Yucatan, the Caribbean coast of Honduras, and Cuba, and drier than average over the rest of the basin, i.e. Costa Rica and northern South America. The following spring, as the atmospheric circulation transitions to normal conditions, the positive SST anomaly that has built up in the basin takes over, favoring convection. The positive precipitation anomaly spreads southeastward, from the northwest to the entire basin. At the start of a new rainy season, it is especially strong over the Greater Antilles.

1. Introduction

Relevant work regarding the large-scale circulation patterns associated with extremely dry or wet conditions in the Caribbean basin dates back to the 1970s, when the sparseness of the data was necessarily compensated by observational insight. Hastenrath (1976, 1978, 1984) averaged normalized rainfall records at 48 stations in Central and northern South America that collected data over the period 1911-1972. He used these as a guide to composite the sea level pressure (SLP) and sea surface temperature (SST) fields over the tropical Atlantic and eastern equatorial Pacific Oceans, for the ten driest and ten wettest summers (July-August) and preceding winters (January-February). Hastenrath observed an anomalously dry summer to be accompanied by lower SLP and higher SST in the equatorial Pacific, unmistakable signature of an ongoing warm ENSO event. At the same time, SLP was higher and SST lower in the tropical Atlantic, an indication of an anomalously strong (or equatorward-displaced) North Atlantic High. It is interesting to note here that the variability within a mean annual cycle is governed by a mechanisms similar to that of interannual variability (Hastenrath, 1984). The secondary rainfall minimum in July-August is, in a mean annual cycle sense, explained in terms of a westward enhancement of the subtropical high. The indication for the winter season preceding a dry summer is for an early southward displacement of the North Atlantic High, and stronger trade winds, along with an equatorward shift of the eastern Pacific ITCZ. The same patterns, with opposite signs, are recovered for the anomalously wet case.

Even though an ENSO signature is unquestionably present in the picture drawn above, ENSO teleconnections with the Caribbean region in the global surveys conducted by Ropelewski

and Halpert (1987, 1989, 1996) and Kiladis and Diaz (1989) present a counterpoint to the strong signals the same authors find in other regions of the tropics, even ones farther away from the eastern Pacific source region. These studies detect a relatively weak tendency toward drier than average conditions in the Caribbean basin from July to October of year (0)[1] of a warm phase of ENSO. It is noted that the signal in the Caribbean basin-Central American region is weaker than the ones in bordering regions. For example, drier than average July of year (0) to March of year (+1) for northeastern South America, and wetter than average October of year (0) to March of year (+1) for the Gulf of Mexico region.

Several recent studies trace teleconnections with ENSO on a subregional scale. As reported by Chen et al. (1997), Jamaica is more likely to experience floods during May to July of year (+1) of a warm phase. Cuba, too (Cardenas and Perez, 1991; Naranjo, 1994; Naranjo, 1997), is more likely to experience excessive rainfall during the late winter (January to March of year (+1)) of a warm ENSO event. This anomaly is attributed to an increased occurrence of disturbances of midlatitude origin. The effect of ENSO can further be complicated by the presence of topography, as in Costa Rica (Waylen et al., 1996). In this last case, the intensification of the trade winds, from the Caribbean basin westward towards the eastern Pacific ITCZ, observed during the summer of year (0) of a warm ENSO event, acts in conjunction with topographic uplift to increase rainfall totals on the Caribbean coast, while simultaneously decreasing them on the Pacific one. In other recent work, Enfield and collaborators (Enfield, 1996; Enfield and Mayer, 1997; Enfield and Alfaro, 1999) investigate the relationship between SST in the Atlantic

[1]The terminology of Rasmusson and Carpenter (1982) is adopted here to indicate the phases of a 'canonical' ENSO cycle. Year (0) is the calendar year that ends with a mature SST anomaly in the central Pacific. Year (+1) is the year immediately following, which starts with the same anomaly.

and Pacific Oceans, and rainfall anomalies in the Caribbean-Central American region. They find a stronger, less equivocal response to SST variability in terms of rainfall when anomalies in the Atlantic and eastern Pacific basins are of opposite signs: when the eastern Pacific is colder and the tropical Atlantic warmer, rainfall anomalies are positive in the Meso-American region. In focusing the attention on SST variability only, Enfield and Mayer (1997) present interesting evidence on the modality with which the two basins interact. They find that anomalies in the tropical Atlantic can be linked to anomalies of the same sign in the eastern Pacific. Warmer than average Atlantic SST, particularly enhanced along the latitudinal band between 10°N and 20°N, west of 40°W, is associated with a reduction in the strength of the Atlantic northeasterly trades. It is also found to follow warm ENSO events with a lag of about a season, and to be most pronounced during the spring. A pattern is thereby proposed in which the tropical North Atlantic and eastern equatorial Pacific are both warm, during a warm ENSO event (or cold, during a cold ENSO event), with the tropical North Atlantic lagging the eastern Pacific by a few months.

The region comprising the Caribbean basin and Central America, between 5°N and 25°N latitude, and 90°W and 60°W longitude, is, precisely because of its geographical position, the natural candidate as the starting point in the investigation of the interaction between the tropical North Atlantic and eastern equatorial Pacific ocean-atmosphere systems. We wish to clarify the role played by the Pacific and Atlantic basins on the seasonality and interannual variability of Caribbean rainfall, our ultimate goal being a better understanding of the tropical teleconnection between ENSO and the Atlantic, and of the modes of climate variability internal to the Atlantic basin. The seasonal cycle of Caribbean rainfall is reviewed in section 3: the application of

Principal Component Analysis to station monthly climatologies permits an objective and succint classification of the spatial and temporal features of the annual cycle of Caribbean rainfall. The study of interannual variability, and its dependence on seasonality, are approached from two complementary points of view. In section 4, canonical correlation analysis (CCA) is used to identify the large-scale patterns of sea level pressure and sea surface temperature that best explain the simultaneous patterns of interannual rainfall variability in the Caribbean-Central American region. Once these patterns are linked to the well-known leading modes of interannual variability, i.e. ENSO on a tropic-wide scale, and the North Atlantic high on a basin-wide scale, an attempt is made to separate the roles of the Pacific and Atlantic basins. This is done, in section 5, by drawing correlation maps of the standard climatological variables, SLP and SST, with indices of the state of the eastern Pacific (NINO3[2]) and Atlantic (North Atlantic High SLP[3]) basins. The analyses in sections 4 and 5 are carried out separately for each two-month period. It is the comparison of consecutive correlation maps that allows the authors to construct a dynamical explanation for the evolution of climate anomalies. A discussion section follows.

2. Data and Methods

a. data

NOAA NCDC GCPS station records of monthly rainfall accumulated (Baker et al., 1994) are analyzed to characterize the seasonal and interannual variability of Caribbean rainfall. We

[2]NINO3 is defined as the average SST in the eastern Pacific box 5°S to 5°N, 150°W to 90°W.

[3]We define SLP averaged over the region between 20°N and 40°N latitude, and 60°W and 30°W longitude, to be our 'North Atlantic High' index.

selected 188 stations located in Central America, the Antilles, and northern South America, on the basis of geographical location and length of record. Only those stations between 5°N and 25°N, and 90°W and 60°W that have at least 25 years (300 months) of data between 1900 and 1995 are kept. From an inspection of the variability in the number of stations collecting data at any time, it is concluded that only the period between 1951 and 1980 provides a spatial coverage sufficient to characterize the climatic variability over the entire basin. With regards to SLP and SST, the results of the reduced-space optimal interpolation technique (Kaplan et al., 1997, 2000) applied to the COADS SLP (Slutz et al., 1985) and MOHSST5 SST (Bottomley et al., 1990) fields are used in the domain comprising latitudes 35°S to 45°N, and longitudes 150°W to 15°E. The entire length of the SLP and SST record (mid-19th century to the present) is used in carrying out the analyses discussed in section 5, whereas canonical correlation analysis (section 4) is restricted to the 1951-80 period common to the rainfall dataset.

All the steps in analysing the interannual variability (subject of sections 4 and 5) are carried out separately for each bimonthly interval (January-February, March-April, May-June, July-August, September-October and November-December). This compromise between monthly mean and seasonal or annual mean calculations is thought to best fit the seasonal variability of the Caribbean basin. It is chosen having in mind the alternation between relative rainfall maxima (in May-June and September-October) and minima (in July-August) during the rainy season.

b. methods

We make extensive use of multivariate analysis techniques (Preisendorfer, 1988; Peixoto and Oort, 1992; von Storch and Navarra, 1995). We apply principal component analysis (PCA) to

the rainfall, SLP and SST fields separately, in order to identify their characteristic patterns of variability over the period common to all datasets (1951-80). We then combine the fields, rainfall and SLP, and rainfall and SST, separately, in canonical correlation analysis (CCA). This allows us to determine patterns of covariability of each of the primary meteorological fields (SLP and SST), with the (presumed) dependent field (rainfall). We follow the procedure described by Barnett and Preisendorfer (1987), also summarized in Bretherton et al. (1992), and applied in Wallace et al. (1992).

In CCA it is common to apply a statistical criterion to retain only as many modes as are necessary to reproduce a certain threshold total variance. Here our foremost interest is to understand the dynamics that link the patterns of SLP and SST to rainfall, and a more stringent criterion is applied. In the SLP-SST case, only those modes recognizable as well-known, large-scale modes of variability are kept; with the exception of SST in July-August, they coincide with those modes that are statistically separable following North's rule (North et al., 1982). In the rainfall case, only those modes that could be statistically separated following North's rule are retained. PCA of rainfall, SLP and SST is performed over the common period (1951-80), and Singular Value Decomposition (SVD) is applied to the leading modes obtained from PCA.

3. Annual cycle of Caribbean rainfall

Climate in the Caribbean basin can be classified as *dry-winter tropical* (Rudloff, 1981), with significant sub-regional variations in annual totals, length of the rainy season and timing of rainfall maxima. The climatological (1951-1980) annual mean rainfall, averaged over all the 188 stations selected, is 1618 millimeters per year. It exceeds 2000 millimeters per year in Costa

Rica and along the Caribbean coast of Honduras, and is less than 600 millimeters per year along the Venezuelan coast west of Caracas, and just north of it, in the Netherlands Antilles. The variance about the mean can be as large as the mean itself.

The salient features of the annual cycle are efficiently summarized by Principal Component Analysis (PCA) of the stations' mean monthly climatologies (Stidd, 1967) (Figure 1). Each station's monthly climatology is normalized locally, by subtracting the station's long-term mean and dividing by its standard deviation. The first three principal components explain 90% of the total variance (66, 14 and 10%, respectively) of the climatological annual cycle. Principal component (PC) 1 (Figure 1, top left) retains the features of the mean Caribbean rainy season, which runs from May to October, with peaks in May-June and September-October, and a relative minimum in July-August. The dry season is centered around the winter months, January to March. Sub-regional variations are clearest when PCs 2 and 3 are linearly combined into their sum (Figure 1, bottom left), or difference (Figure 1, bottom right). Three rainfall 'regimes' can be related to the geography of the Caribbean-Central American region (Figure 1, right column). A *May to October* rainfall regime, when the spatial loading associated with the difference between PCs 2 and 3 is negative, is typical of the Central American stations, and of the South American stations east of the Cordillera de Merida in Venezuela. A regime characterized by a pronounced *mid-summer break* in rainfall accumulations, when projection onto the difference between PC 2 and PC 3 is positive, is typical of the interior of the basin, i.e. the southern coasts of Jamaica and Hispaniola, and northwestern South America. A regime characterized by a *late-fall peak* in rainfall, when projection onto the sum of PC 2 and PC 3 is positive, is typical of the Caribbean coast of Honduras, as well as the northern coasts of Jamaica and Hispaniola, of Puerto Rico and

of the Lesser Antilles.

The picture just drawn is the result of the interaction between the complex topography, made up of island chains and mountain ranges with varying orientations, and the large-scale atmospheric circulation of a region that spans the deep tropics as well as the subtropics. Subsidence, which is associated with the spreading of the subtropical high from the Atlantic Ocean to the cool North American land mass, dominates the Caribbean basin during the winter, or dry season. Polar fronts of mid-latitude origin regularly invade the region, contributing to rainfall totals over the northwestern part of the basin. In late spring (late April-early May), as the subtropical high moves back off-shore, the circulation pattern characteristic of the rainy season kicks in, with easterly winds dominating over the entire basin, from the surface up into the upper troposphere. Rainfall-bearing disturbances, known as African easterly waves (Riehl, 1945; Burpee, 1972), propagate across the Atlantic Ocean into the Caribbean basin from mid-June to early October (Burpee, 1972). On the eastern Pacific side, rainfall is associated with the meridional migration of the ITCZ. The annual component of such migration dominates over the semiannual one (Mitchell and Wallace, 1992), and the effect is to strongly favor the northern hemisphere in terms of total rainfall amount. Once the ITCZ has moved off the equator to the north, after the spring equinox, feedback mechanisms between the converging trade winds and SST maintain it to the north of the equator through the fall equinox (Mitchell and Wallace, 1992). This convergence of moisture toward the northern hemisphere, from July to October, constitutes the Central American monsoon.

To summarize the description of the large-scale atmospheric circulation surrounding the Caribbean, and its effect in terms of rainfall: conditions favorable to convection (warm SST, deep,

unstable boundary layer, easterly propagation of disturbances, convergence of winds toward the basin from both sides, Atlantic and Pacific) dominate the region during the warm season (May to October). The mid-summer break is associated with the temporary intensification of the North Atlantic High (Portig, 1965; Hastenrath, 1976), which strengthens subsidence over the basin (Knaff, 1997). During the cold season (November-April) subsidence dominates the region, stifling convection. With the exception of the 'northwestern corner', which is affected by extratropical climate variability during this time of the year, this results in a dry winter season.

4. The influence of Atlantic and Eastern Pacific climate variability on Caribbean rainfall

a. principal component analysis of SLP, SST and rainfall

As previewed in section 2, SLP, SST and rainfall are pre-filtered by means of PCA, computed over the years 1951-80, prior to the application of SVD. The total variance explained by the SLP, SST, and rainfall principal components selected is summarized in Table 1.

PC 1 of SLP strongly correlates with the NINO3 index, for all bimonthly intervals except January-February (cf. Table 2, column 1, for the correlation values). The associated spatial pattern (not shown) resembles a zonal seesaw between the tropical latitudes of the eastern Pacific and Atlantic basins: when SLP is anomalously low over the equatorial eastern Pacific, it is anomalously high over the equatorial Atlantic. PC 2 of SLP is a tropical Atlantic mode. It correlates significantly with SLP averaged between 15°S and 15°N latitude, and 60°and 30°W longitude (cf. Table 2, column 2). PC 3 of SLP (not shown) is an extratropical Atlantic mode:

it more clearly projects onto the region comprised between 20°N and 40°N (cf. Table 2, column 3), tracking the seasonal migration of the subtropical high.

PC 1 of SST (not shown) is an ENSO mode for the July-August to January-February intervals (cf. Table 3, column 1, for the correlation values). The correlation is weaker during the March to June transitional period. During May-June, PC 1 correlates with NINO3 (0.55), as well as with the tropical Atlantic dipole index (0.54). PCs 2 and 3 of SST (not shown) also correlate with the tropical Atlantic dipole index (cf. Table 3, columns 2 and 3), especially during the summer months (May-June to September-October). The tropical Atlantic dipole index, sometimes referred to as the tropical Atlantic SST index (Moura and Shukla, 1981; Servain and Merle, 1993; Chang et al., 1997), is defined here as the difference between the SST anomalies averaged over 5°N to 25°N and 60°W to 15°E, and over 20°S to 5°N and 60°W to 15°E. A dipolar pattern, with SST anomalies of contrasting sign in the tropical latitudes of the North and South Atlantic, is recurrent in Principal Component Analyses of SST (e.g. Houghton and Tourre, 1992), and, in particular, in combined analyses of Atlantic SST and rainfall over the continental regions bordering it, e.g. Northeast Brazil (Moura and Shukla, 1981) and the Sahel (Lamb et al., 1986; Palmer, 1986). However, its physical existence and relevance to interannual climate variability in the Atlantic sector is currently being vigorously questioned. Even though a seductive mechanism for a dipolar oscillation has been proposed (Chang et al., 1997), recent research (Houghton and Tourre, 1992; Enfield and Mayer, 1997; Enfield et al., 1998; Rajagopalan et al., 1998; Mehta, 1998) finds little evidence for a coherent tropical Atlantic signal.

Because Caribbean station rainfall is restricted to 30 years of data in order to recover a sufficient spatial coverage of the Antilles, Central and northern South America, only the first

two modes are separable according to North's rule (North et al., 1982). The leading mode (not shown) is relatively homogeneous throughout the basin, with interesting contrasting signatures on the Caribbean coasts of Yucatan, Honduras and Costa Rica. In particular, the northern coasts of Yucatan and Honduras have signature opposite to the rest of the basin in November-December and January-February, whereas the Caribbean coast of Costa Rica has signature opposite to the Pacific coast in July-August and September-October. In pattern 2 (not shown), the stations exhibit a tendency to cluster on a sub-regional scale. Recurrent clusters are formed by the islands of Jamaica, Hispaniola and Puerto Rico, by Costa Rica, by the Pacific coast of Central America, by northern Honduras, and by northeastern South America.

b. canonical correlation analysis

CCA is computed using the first three SLP or SST modes, and the first two rainfall modes. Together, these modes explain about 60% (SLP), 45% (SST), and 30% (rainfall) of the total variance of the respective fields. Results are displayed in figures 2 (SLP and rainfall) and 3 (SST and rainfall), in terms of *heterogeneous* correlation maps. We show only those pairs with CCA time coefficients that correlate above 0.35 or better, which is statistically significant at the 95% level (cf. Table 4).

The two SLP patterns obtained from CCA (Figure 2 and see Table 5) can be broadly characterized as an inter-basin mode, and an Atlantic mode. The inter-basin mode is a zonal oscillation, or seesaw, between the Atlantic and eastern Pacific basins. When SLP over the eastern equatorial Pacific is lower than average, it is higher than average over the tropical North Atlantic, a pattern associated with negative rainfall anomalies for the bimonthly periods of July-

August to January-February. We will return to the dynamical interpretation of the seesaw pattern in the next section. The Atlantic mode is statistically significant only in the two-month periods of July-August, November-December, and January-February. It can be interpreted to affect rainfall by influencing the direction of the moisture fluxes in the region surrounding the Caribbean, as well as subsidence directly above it. When, as in July-August, the positive SLP anomaly is over the Caribbean, the Gulf of Mexico and North America, rainfall anomalies in the Caribbean are generally negative. A plausible explanation, first given by Hastenrath (1976), is that higher than average SLP in the western North Atlantic region is associated with anomalously strong subsidence over the basin. The notable exception in this picture is the Caribbean coast of Costa Rica: there, rainfall anomalies are positive, possibly a topographic effect, as argued by Waylen et al. (1996). Higher-than-average SLP off the east coast of North America, as in November-December (not shown), can be interpreted as steering the Atlantic moisture flux away from the Caribbean toward the northwest, and is thus also associated with negative rainfall anomalies. Lower-than-average SLP over the same region in the wintertime (January-February, not shown) is seen to increase the moisture flux from the extratropical regions towards the northern portion of the Caribbean, and is associated with positive rainfall anomalies over the Greater Antilles.

In the case of CCA of SST and rainfall (cf. Figure 3 and Table 5), the recurrent patterns are the tropical Atlantic SST dipole, with somewhat stronger loading onto the North Atlantic, and ENSO. Percentages of the total variance of rainfall explained are shown in Table 5. The ENSO mode is present during the second half of the rainy season, in July-August, and September-October (not shown): a warm eastern Pacific SST is associated with negative rainfall anomalies in the Caribbean. In November-December (not shown) and January-February, a positive tongue

of warm waters extends from the eastern Pacific into the Caribbean-western Atlantic basin. This situation resembles the warming of tropical north Atlantic waters, delayed by about a season with respect to the Pacific El Niño-related warming, as described by Pan and Oort (1983) and Enfield and Mayer (1997). It is associated with strong negative rainfall anomalies over the southern part of the region, in northern South America and Costa Rica, and weaker positive anomalies limited to the northwestern corner of the basin, in November-December, and extending to the Antilles, in January-February. The only statistically significant mode in May-June bears a strong resemblance to the tropical Atlantic dipole; its PC correlates to 0.93 with the tropical Atlantic dipole index. A warm tropical North Atlantic, from West Africa to the Caribbean, is associated with positive rainfall anomalies in our region of interest. Circum-Atlantic rainfall variability is known to be sensitive to meridional gradients in SST, as exemplified by the tropical Atlantic dipole pattern. Rather than interpreting the dipole pattern as the physical pattern affecting rainfall, an alternative interpretation is emerging (Enfield et al., 1998; Rajagopalan et al., 1998), which views meridional gradients in surface temperature as the relevant variable, to be related to rainfall variability. The same SST pattern can also be interpreted as the natural follow-up to the ENSO-related patterns described for the two-month periods preceding the spring season. (The correlation between the same time coefficient and the December(0)-January(+1) NINO3 is 0.49). The warming in the western Atlantic lags the Pacific warming by about a season, peaking during the spring after the mature phase of ENSO. It is related to positive rainfall anomalies in the Caribbean at the start of a new rainy season, as well as to concomitant negative rainfall anomalies in the northeastern region of Brazil (Nobre and Shukla, 1996). The ENSO-related warming will be more thoroughly discussed in the next section.

5. ENSO and the Atlantic Ocean

In this section we follow a strategy complementary to the one carried out in the previous one. An attempt is made to single out the contribution of each basin to the state of the ocean-atmosphere system affecting Caribbean rainfall. The NINO3 index is used as a proxy for eastern Pacific climate variability, the North Atlantic High index (see the previous section for a definition) as a proxy for Atlantic climate variability. These indices are chosen as a logical consequence of the CCA results just described. They represent the leading modes of interannual climate variability in the Pacific and Atlantic basin, respectively.

A 'canonical' cycle of the influence of ENSO on the tropical Atlantic basin can be described by means of correlation maps of sea level pressure, and sea surface temperature with the NINO3 index, computed over the 130-year period going from 1861 to 1990. The SLP and SST anomalies averaged over the bimonthly intervals from July-August of year (0) to May-June of year (+1) are correlated against the 'mature' NINO3 value, i.e. NINO3 averaged over December(0)-January(+1). Results are shown in figure 4 for the two-month periods of July-August (0), January-February (+1), and May-June (+1). In order to understand the dynamics that underlie the development of persistent SST anomalies in the Caribbean-western Atlantic region (Pan and Oort, 1983; Hastenrath et al., 1987; Enfield and Mayer, 1997) well after the ENSO event has subsided in the equatorial Pacific, it is useful to focus first on the atmospheric variables. Correlation maps of sea level pressure with December(0)-January(+1) NINO3, indicate the development of a coherent anomalous circulation pattern from as early as July-August (0): in response to an anomalously low SLP in the eastern Pacific, that epitomizes the shift in

convergence patterns characteristic of a warm event, SLP is anomalously high over the equatorial Atlantic. This anomaly in SLP closely resembles the 'zonal seesaw' mode described in the preceding section. It is consistent with a weaker-than-average meridional SLP gradient between the North Atlantic subtropical high and the ITCZ, hence weaker-than-average easterly winds in the tropical latitudes of the North Atlantic. Decreased surface easterlies translate into decreased loss of heat from the ocean to the atmosphere, hence increased SST. The increase in SLP over the tropical Atlantic is recognizable in correlation maps from July-August (0) to March-April (+1) (not shown), and is particularly strong during the winter months, e.g. January-February (+1). During these months the positive SLP anomaly center gradually shifts to the South Atlantic. This happens in conjunction with the establishment of a wave-train-like pattern, reminiscent of the Pacific-North American (PNA) teleconnection pattern (Wallace and Gutzler, 1981; Horel and Wallace, 1981; Hoskins and Karoly, 1981). The center of action off the coast of the southeastern United States, a negative SLP anomaly, is most prominent in the January-February (+1) and March-April (+1) maps . The presence of such a center acts to enhance the weakening of the trade winds in the North Atlantic, and to displace the positive SLP anomaly to the south of the equator.

To clarify the association between SLP anomalies and the anomalous surface circulation, we also analyze SLP and surface wind data from the NCEP-NCAR Reanalysis Project (Kalnay et al., 1996). The correlation maps in Figure 5 are taken over a shorter time interval (1958 to 1997), but the same SLP patterns as during the 1861-1990 period are reproduced. The seesaw in SLP is clearly identifiable (contoured in Figure 5), both in the July-August (0) and January-February (+1) intervals. So is the negative SLP anomaly center off the east coast of North America during

the winter and spring. These anomalies are associated with a strong dipole in divergence over the eastern and central equatorial Pacific, with convergence along the equator and divergence to the north of it, between 5°N and 15°N. Divergence extends to the east into the Caribbean basin, in July-August (0). (Note the small region of convergence on the Caribbean side of Costa Rica, in agreement with Waylen et al. (1996)). It is strong over the basin and to the east of it, along the northern coast of South America, in January-February. At this time, convergence is noticeable to the north of the basin, in the Gulf of Mexico, in association with the low SLP center off the east coast of North America. By the start of the next rainy season, in May-June (+1), SLP is anomalously low over the basin, and convergence has extended from the Gulf of Mexico into the Caribbean. In terms of wind anomalies, divergence away from the Caribbean basin, along a northeast-southwest axis, is evident in the July-August (0) and January-February (+1) correlation maps. Then, the cyclonic circulation around the negative SLP anomaly intensifies, and follows the convergence pattern into the Caribbean basin.

As the ENSO event dies down, during spring (+1), the anomalies in the atmospheric circulation quickly adjust to the newly established conditions. But the SST anomalies, particularly the positive (in the case of a warm event) anomaly in the western tropical North Atlantic, persist beyond the event. The correlation of SST with December(0)-January(+1) NINO3 is still greater than 0.6 in the entire Caribbean basin during March-April (not shown) and May-June of year (+1), period during which it peaks. We hypothesize that this SST anomaly is responsible for the positive rainfall anomaly that we notice in the spring following an ENSO event, in a trend contrasting the anomalous patterns preceding the mature ENSO phase. The SST anomaly is also pointwise statistically significant at the 99% confidence level (assuming the points in the

130-year-long time series to be independent, since the correlation is computed separately for all bimonthly periods) in the entire tropical North Atlantic: a secondary maximum can be noticed along the coasts of the west African states of Guinea and Sierra Leone. The correlation then weakens from July-August (+1) onwards, but its characteristic pattern (not shown), with three maxima, in the Caribbean, western South Atlantic, and off the coast of Guinea, is still present in November-December (+1) maps.

Turning to the Atlantic sector (see Figure 6) and starting from the winter months, when large-scale atmospheric patterns in general show greater persistence, we observe the correlation of the December-to-March North Atlantic High index with SLP to rapidly decrease during the transition from winter to spring. We find, in agreement with Hastenrath (1976), a return to significant correlation values in the tropical western Atlantic between the December-to-March index and SLP in July-August. Higher than average wintertime SLP in the subtropical North Atlantic region is an indication of higher than average western tropical North Atlantic SLP the following summer, the correlation being greater than 0.3 over the entire Caribbean basin/Gulf of Mexico region, with maximum values of over 0.4 to the north of the Greater Antilles. The correlation patterns of the North Atlantic High index with SST strongly resemble a 'sandwich pattern, with band anomalies of one polarity over the western ocean, centered near 30°- 35°N, flanked by anomalies of the opposite polarity over the northern ocean, near 50°N (not captured in our analysis), and in the subtropics, near 15°N' (Wallace et al., 1990). In particular, the negative correlation between the North Atlantic High index and SST in the tropical belt, between the equator and 25°N, persists from the winter into the following rainy season, with maximum values, of the order of 0.4 or greater, around 15°N, 60°W. The anomalous anticyclonic circulation, and

the anomalous SSTs can be linked together (e.g., Wallace et al., 1990; Cayan, 1992; Delworth, 1996). The positive SST anomaly in the Gulf Stream region can be explained in terms of the anomalous northward advection of warm, moist air, to a colder ocean region, resulting in reduced evaporation, hence an SST warming. The negative SST anomalies to the north and south can be explained in terms of stronger surface winds, westerly and easterly, respectively, and increasing evaporation leading to SST cooling. However, it is difficult to separate the impact of thermodynamic processes and of advection of SST by anomalous wind-driven currents. In summary, a stronger than average North Atlantic High during the winter, or dry season, translates into cooler tropical North Atlantic waters, hence negative Caribbean rainfall anomalies, during the following summer, or rainy season.

To test the connections between SLP and SST patterns over the eastern Pacific and Atlantic oceans, and rainfall in the Caribbean basin, correlations between the climate indices suggested by the analysis above, i.e. NINO3, and the North Atlantic High index, and station rainfall, were computed for the 1951-1980 interval. The correlation patterns are very similar to the rainfall patterns of CCA presented in Figures 2 and 3. Correlations of the December(0)-January(+1) NINO3 index with rainfall, are negative over the entire basin during the July to October months preceding the mature phase, in agreement with Ropelewski and Halpert (1987) and Kiladis and Diaz (1989), with the exception of the Caribbean coast of Costa Rica, thus confirming what found locally by Waylen et al. (1996). They are strongest, negative over northern South America and the Caribbean coast of Honduras, and positive over Cuba, during November to February. The positive correlation then spreads out from the northwestern corner to cover the entire basin in late spring, in agreement with Chen et al. (1997). Correlations with the

December-March North Atlantic High index are negative, and strongest during the May-June following the winter, over the Antilles and northeastern South America, when the correlation between the North Atlantic High index and SST is also strongest negative, i.e. less rainfall is associated with cooler western Atlantic SST, brought about by a stronger North Atlantic High. Negative correlations persist into July-August.

6. Discussion and Conclusions

We started this study with a canonical correlation analysis between rainfall over the Caribbean region (90°W to 60°W, and 5°N to 25°N), and sea level pressure and sea surface temperature over the eastern Pacific and Atlantic Oceans (150°W to 15°E, 35°S to 45°N), for the years 1951-1980. We found that about 30% of the total variance in rainfall in this region can be explained in terms of the interannual climate variability of either Pacific (i.e. ENSO), or Atlantic (i.e. North Atlantic subtropical high), source, and their related changes in tropical Atlantic SST. The CCA results pointed to NINO3 and the strength of the North Atlantic High as the climatic indices relevant to Caribbean rainfall variability. We correlated these indices with sea level pressure and sea surface temperature and obtained a coherent picture of the evolution of the ENSO teleconnection to the Atlantic sector.

ENSO manifests itself in the tropical atmosphere as a zonal seesaw in SLP between the eastern equatorial Pacific and Atlantic oceans. We hypothesize that the interaction between the two basins takes place primarily through an anomalous Walker circulation, set up by the eastward shift of the convectively active region in the Pacific. This involves ascent over the eastern Pacific and descent over the equatorial Atlantic. When SLP over the unusually warm

waters of the central Pacific is lower than average, it tends to be higher than average over the equatorial Atlantic, with the Caribbean constituting the boundary between negative and positive SLP anomalies. This seesaw pattern has a direct effect on convergence in the Caribbean basin. When SLP is higher than average in the Atlantic, and lower than average in the eastern Pacific, the atmospheric flow at the surface is divergent over the Caribbean basin, along a southwest-to-northeast axis, with convergence onto the eastern Pacific ITCZ, to the west, and into the tropical North Atlantic, to the east. Hence the reduction of local moisture flux convergence. The same anomalous SLP pattern also has an indirect effect on SST. This is lagged by about a season, and peaks when the ENSO event has died down, in the spring following the mature phase: higher than average SLP in the region of the Atlantic ITCZ decreases the meridional SLP gradient, hence decreasing wind speeds in the trade wind belt, reducing evaporation and increasing SST. In addition to the tropical 'seesaw' in SLP, the effect of ENSO is indirectly communicated to the Atlantic basin through the midlatitudes of the North American continent, by a wave-train pattern, reminiscent of the PNA, in an alternance of high and low pressure centers. This pattern terminates with anomalously low SLP (during a warm event), in the subtropical western Atlantic: the relationship between it and the subtropical North Atlantic high remains one of the subjects in need of further investigation.

The Caribbean is caught between the Gulf of Mexico, which is wetter than average during warm ENSO events, and northern South America, which is drier (Ropelewski and Halpert, 1987, 1989, 1996), and takes on characteristics of both regions during different phases of an event. We identify three actors: the tropical (seesaw) and extratropical (PNA-like) atmospheric responses to the Pacific warming, and the lagged ocean response in the tropical North Atlantic. These re-

sponses have contrasting effects on Caribbean-Central American rainfall. Divergence, due to the tropical 'seesaw', translates into dry conditions, starting from July of year (0). The extratropical 'PNA-like' response, strongest during the winter season, is associated with low pressure, convergence, and rain, which gradually migrate from the Gulf of Mexico to the Caribbean. Finally, the ocean response, a lagged warming of Caribbean-western Atlantic waters, favors convection over the region during the spring which follows a warm ENSO event.

Atlantic climate variability, as exemplified by the role of the North Atlantic High, also is able to excite Caribbean rainfall variability. On this side of our domain of interest, atmospheric anomalies typically persist no longer than a season. An intriguing sign of atmospheric persistence is the positive correlation between SLP during the winter months, and SLP halfway through the Caribbean rainy season, in July-August, when an intensification of the subtropical high shapes the break in the rainfall patterns (Hastenrath, 1976). On the other hand, we find Atlantic SST anomalies excited by the SLP anomalies to persist on a time scale longer than one season. In particular, SST anomalies excited during the winter-early spring period, are shown to last through the following rainy season. Higher than average SLP over the North Atlantic High region (60°W to 30°W, 20°N to 40°N) is associated with positive SST anomalies off the eastern coast of North America, straddled by negative anomalies to the north and south. The negative SST anomalies in the tropical North Atlantic are associated with negative Caribbean rainfall anomalies.

With regards to the prediction of climate on a seasonal to interannual timescale, two aspects highlighted by this work seem relevant. First of all, the notion that atmospheric anomalies, whether originated in the mid-latitudes of the North Atlantic basin, or the equatorial

latitudes of the Pacific basin, can affect tropical and Caribbean climate by exciting persistent SST anomalies, and in turn affect the local atmospheric conditions. Secondly, to the extent that Atlantic and Pacific climate variability are independent, their effect on Caribbean climate can add up in a positive or negative interference pattern: a warm ENSO event and lower than average North Atlantic High SLP are both capable of generating positive tropical North Atlantic SSTs, thus positive Caribbean rainfall anomalies. A strong North Atlantic High, as in a positive NAO (North Atlantic Oscillation) phase, can potentially cancel the warming effect on SSTs of a warm ENSO event. One aspect that remains to be discussed is the extent to which a warm ENSO event can precondition North Atlantic SLP, either in favor of lower-than-average SLP in the wintertime, or by shifting the high SLP center to the east, as shown by correlation maps. To the extent that significant dry or wet anomalies can be timed with respect to the evolution of a 'canonical' ENSO event, the correlation between ENSO and the state of the Caribbean ocean-atmosphere system can be exploited in a forecasting mode of operation (Hastenrath, 1995). The same obviously cannot be said for the Atlantic basin. On this side of the Caribbean, more research is needed to advance our understanding of the tropical ocean-atmosphere, as well as tropical-extratropical, interaction, and of the mechanisms of decadal variability.

Acknowledgments. This work was supported by the National Oceanic and Atmospheric Administration under grant NA56GPO221. We wish to thank John Chiang, Amy Clement, Heidi Cullen, Mike Evans, Balaji Rajagopalan, Alexey Kaplan, Steve Zebiak, Richard Seager, and Paulo Nobre for their encouragement, and for the time dedicated to discussions. Special thanks go to Benno Blumenthal for his support in handling the data through the IRI/LDEO

Climate Group Data Library website (http://rainbow.ldeo.columbia.edu/), and to Larry Rosen and Virginia Di-Blasi Morris, for their technical support. Many thanks are due to the editor, Neville Nicholls, who accomplished his duty expeditiously and gracefully, and to the reviewers, David Enfield and Stefan Hastenrath; their requests to clarify and sharpen the content of the paper were of great help to the authors.

References

Baker, C. B., Eischeid, J. K., Karl, T. R., and Diaz, H. F., 1994: The quality control of long-term climatological data using objective data analysis. *Preprints of AMS Ninth Conference on Applied Climatology, Dallas, TX., January 15-20, 1995.*

Barnett, T. P. and Preisendorfer, R. W., 1987: Origins and levels of monthly and seasonal forecast skill for United States surface air temperatures determined by canonical correlation analysis. *Mon. Wea. Rev.*, **115**, 1825–1850.

Bjerknes, J., 1964: Atlantic air-sea interaction. *Advances in Geophysics*, **10**, 1–82.

Bottomley, M., Folland, C. K., Hsiung, J., Newell, R. E., and Parker, D. E., 1990: Global ocean surface temperature atlas "GOSTA". Meteorological Office, Bracknell, UK and the Department of Earth, Atmospheric and Planetary Sciences, Massachusetts Institute of Technology, Cambridge, MA, USA. 20 pp and 313 plates.

Bretherton, C. S., Smith, C., and Wallace, J. M., 1992: An intercomparison of methods for finding coupled patterns in climate data. *J. Climate*, **5**, 541–560.

Bunker, A. F., Haurwitz, B., Malkus, J. S., and Stommel, H., 1949: Vertical distribution of temperature and humidity over the Caribbean Sea. pp. 1–82. Papers in Phys. Oceanogr. and Met. published by Mass. Inst. Tech. and Woods Hole Oceanogr. Inst.

Burpee, R. W., 1972: The origin and structure of easterly waves in the lower troposphere of North Africa. *J. Atmos. Sci.*, **29**, 77–90.

Cardenas, P. and Perez, M., 1991: Eventos ENOS y anomalias de las lluvias en Cuba. *Tech. Rep.* Instituto de Meteorologia, Havana, Cuba, 24 pp.

Cayan, D. R., 1992: Latent and sensible heat flux anomalies over the northern oceans: the connection to monthly atmospheric circulation. *J. Climate*, **5**, 354–369.

Chang, P., Link, J., and Li, H., 1997: A decadal climate variation in the tropical Atlantic Ocean from thermodynamic air-sea interactions. *Nature*, **385**, 516–518.

Chen, A., Roy, A., McTavish, J., Taylor, M., and Marx, L., 1997: Using SST anomalies to predict flood and drought conditions for the Caribbean. *COLA Rep.*, **49**. Available from the Center for Land-Ocean-Atmosphere Studies, 4041 Powder Mill Road, Suite 302, Calverton, MD 20705-3106, U.S.A.

Delworth, T. L., 1996: North Atlantic interannual variability in a coupled ocean-atmosphere model. *J. Climate*, **9**, 2356–2375.

Eltahir, C. K. and Gong, C., 1996: Dynamics of wet and dry years in West Africa. *J. Climate*, **9**, 1030–1042.

Enfield, D. B., 1996: Relationship of inter-American rainfall to tropical Atlantic and Pacific SST variability. *Geophys. Res. Lett.*, **23**, 3305–3308.

Enfield, D. B. and Alfaro, E. J., 1999: The dependence of Caribbean rainfall on the interaction of the tropical Atlantic and Pacific Oceans. *J. Climate*, **12**, 2093–2103.

Enfield, D. B. and Mayer, D. A., 1997: Tropical Atlantic sea surface temperature variability and its re lation to El Niño-Southern Oscillation. *J. Geophys. Res.*, **102**, 929–945.

Enfield, D. B., Mestas-Nuñez, A. M., Mayer, D. A., and Cid-Serrano, L., 1999: How ubiquitous is the dipole relationship in the tropical Atlantic sea surface temperatures? *J. Geophys. Res.*, **104(C4)**, 7841–7848.

Hastenrath, S., 1968: A contribution to the wind conditions over the Caribbean Sea and Gulf of Mexico. *Tellus*, **XX-1**, 162–178.

Hastenrath, S., 1976: Variations in low-latitude circulation and extreme climatic events in the tropical Americas. *J. Atmos. Sci.*, **33**, 202–215.

Hastenrath, S., 1978: On the modes of tropical circulation and climate anomalies. *J. Atmos. Sci.*, **35**, 2222–2231.

Hastenrath, S., 1984: Interannual variability and annual cycle: mechanisms of circulatio n and climate in the tropical Atlantic sector. *Mon. Wea. Rev.*, **112**, 1097–1107.

Hastenrath, S., 1995: Recent advances in tropical climate prediction. *J. Climate*, **8**, 1519–1532.

Horel, J. D. and Wallace, J. M., 1981: Planetary scale atmospheric phenomena associated with the Southern Oscillation. *Mon. Wea. Rev.*, **109**, 813–829.

Hoskins, B. J. and Karoly, D., 1981: The steady response of a spherical atmosphere to thermal and orogr aphic forcing. *J. Atmos. Sci.*, **38**, 1179–1196.

Houghton, R. W. and Tourre, Y. M., 1992: Characteristics of low frequency sea surface temperature fluctuations in the tropical Atlantic. *J. Climate*, **5**, 765–771.

Kalnay, E. and Coauthors, 1996: The NCEP-NCAR 40-year reanalysis project. *Bull. Amer. Meteor. Soc.*, **77**, 437–471.

Kaplan, A., Kushnir, Y., and Cane, M. A., 2000: Reduced space optimal interpolation of historical marine sea level pressure: 1854-1992. *J. Climate*, **13**, 2987–3002.

Kaplan, A., Kushnir, Y., Cane, M. A., and Blumenthal, M. B., 1997: Reduced space optimal analysis for historical datasets: 136 years of Atlantic sea surface temperatures. *J. Geophys. Res.*, **102**, 27,835–27,860.

Kiladis, G. N. and Diaz, H. F., 1989: Global climatic anomalies associated with extremes in the Southe rn Oscillation. *J. Climate*, **2**, 1069–1090.

Knaff, J. A., 1997: Implications of summertime sea level pressure anomalies in the tropical Atlantic region. *J. Climate*, **10**, 789–804.

Kushnir, Y., 1994: Interdecadal variations in the North Atlantic sea surface temperature and associated atmospheric conditions. *J. Climate*, **7**, 141–157.

Kushnir, Y. and Held, I., 1996: Equilibrium atmospheric response to North Atlantic sst anomalies. *J. Climate*, **9**, 1208–1220.

Lamb, P. J., Peppler, R. A., and Hastenrath, S., 1986: Interannual variability in the tropical Atlantic. *Nature*, **322**, 238–240.

Mehta, V. M., 1998: Variability of the tropical ocean surface temperatures at decadal-multidecadal timescales. Part I: the Atlantic. *J. Climate*, **11**, 2351–2375.

Mitchell, T. P. and Wallace, J. M., 1992: The annual cycle in equatorial convection and sea surface temperature. *J. Climate*, **5**, 1140–1156.

Moura, A. D. and Shukla, J., 1981: On the dynamics of droughts in northeast Brazil: observations, theory and numerical experiments with a general circulation model. *J. Atmos. Sci.*, **38**, 2653–2675.

Naranjo, L., 1994: Indices de circulacion atmosferica en las immediaciones de Cuba. *Research Report*. Instituto de Meteorologia, Havana, Cuba.

Naranjo, L., 1997: Impacts of ENSO on Cuba. Contribution to 'A systems approach to ENSO', A Colloquium on El Niño-Southern Oscillation (ENSO): Atmospheric, Oceanic, Societal, Environmental, and Policy Perspectives. Held at NCAR, Boulder, Colorado, 20 July - 1 August 1997.

Nobre, P. and Shukla, J., 1996: Variations of sea surface temperature, wind stress, and rainfall over the tropical Atlantic and South America. *J. Climate*, **9**, 2464–2479.

North, G. R., Bell, T. L., Cahalan, R. F., and Moeng, F. J., 1982: Sampling errors in the estimation of empirical orthogonal functions. *Mon. Wea. Rev.*, **110**, 699–706.

Palmer, T. N., 1986: Influence of the Atlantic, Pacific and Indian Oceans on Sahel rainfall. *Nature*, **322**, 251–253.

Palmer, T. N. and Sun, Z., 1985: A modelling and observational study of the relationship between sea surface temperature in the northwest Atlantic and the atmospheric general circulation. *Quart. J. Roy. Meteor. Soc.*, **111**, 947–975.

Pan, Y. H. and Oort, A. H., 1983: Global climate variations connected with sea surface temperature a nomalies in the eastern equatorial Pacific Ocean for the 1958-73 period. *Mon. Wea. Rev.*, **111**, 1244–1258.

Peixoto, J. P. and Oort, A. H., 1992: Physics of Climate. American Institute of Physics, New York.

Portig, W. H., 1965: Central American Rainfall. *The Geophysical Review*, **55**, 68–90.

Preisendorfer, R. W., 1988: Principal component analysis in meteorology and oceanography. p. 418 pp. C. Mobley, Ed., Elsevier.

Rajagopalan, B., Kushnir, Y., and Tourre, Y. M., 1998: Observed decadal midlatitude and tropical Atlantic climate. *Geophys. Res. Lett.*, **25**, 3967–3970.

Rasmusson, E. M. and Carpenter, T. H., 1982: Variations in tropical sea surface temperature and surface wind fi elds associated with the Southern Oscillation/El Niño. *Mon. Wea. Rev.*, **110**, 354–384.

Riehl, H., 1945: Waves in the easterlies and the polar front in the tropics. Misc. Rept., No. 17, Dept. Meteorology, University of Chicago, 79pp.

Ropelewski, C. F. and Halpert, M. S., 1987: Global and regional precipitation patterns associated with the E l Niño/Southern Oscillation. *Mon. Wea. Rev.*, **115**, 1606–1626.

Ropelewski, C. F. and Halpert, M. S., 1989: Precipitation patterns associated with the high index phase of the Southern Oscillation. *J. Climate*, **2**, 268–284.

Ropelewski, C. F. and Halpert, M. S., 1996: Quantifying Southern Oscillation-precipitation relationships. *J. Climate*, **9**, 1043–1059.

Rudloff, W., 1981: World-Climates, with tables of climatic data and practical suggestions. Wissenschaftliche Verlagsgesellschaft mbH Stuttgart.

Servain, J. and Merle, J., 1993: Interannual climate variations over the tropical Atlantic Ocean. 'Prediction of interannual climate variations', NATO ASI Series, vol. 16, J. Shukla, ed. . Springer-Verlag.

Slutz, R. J., Lubker, S. J., Hiscox, J. D., Woodruff, S. D., Jenne, R. L., Steurer, P. M., and Elms, J. D., 1985: Comprehensive Ocean-Atmosphere Data Set; Release 1. Climate Research Program, Boulder, Colorado.

Stidd, C. K., 1967: The use of eigenvectors for climatic estimates. *J. App. Meteor.*, **6**, 255–264.

von Storch, H. and Navarra, A., 1995: Analysis of climate variability. Springer-Verlag, 352 pp.

Wallace, J. M. and Gutzler, D. S., 1981: Teleconnections in the geopotential height field during the northern hemisphere winter. *Mon. Wea. Rev.*, **109**, 784–812.

Wallace, J. M., Smith, C., and Bretherton, C. S., 1992: Singular value decomposition of wintertime sea surface temperature and 500-mb height anomalies. *J. Climate*, **5**, 561–576.

Wallace, J. M., Smith, C., and Jiang, Q., 1990: Spatial patterns of atmosphere-ocean interaction in the northern winter. *J. Climate*, **3**, 990–998.

Waylen, P. R., Caviedes, C. N., and Quesada, M. E., 1996: Interannual variability of monthly precipitation in Costa Rica. *J. Climate*, **9**, 2606–2613.

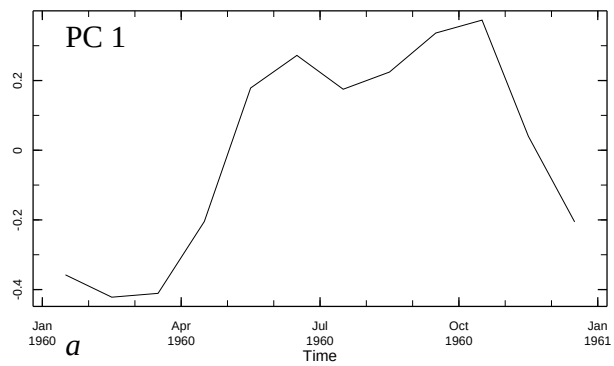
PC 1
0.2
0
-0.2
-0.4
Jan 1960
Apr 1960
Jul 1960
Oct 1960
Jan 1961
Time

a

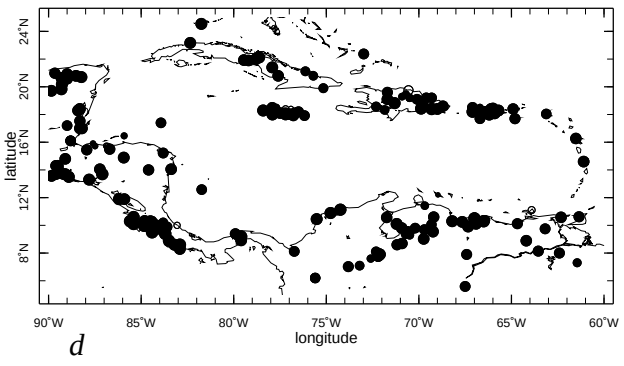
24°N
20°N
16°N
12°N
8°N
latitude
90°W
85°W
80°W
75°W
70°W
65°W
60°W
longitude

d

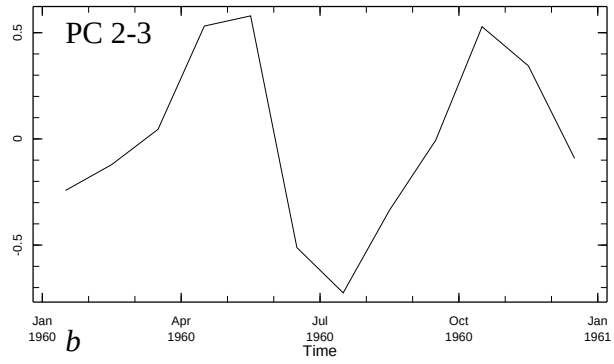
PC 2-3
0.5
0
-0.5
Jan 1960
Apr 1960
Jul 1960
Oct 1960
Jan 1961
Time

b

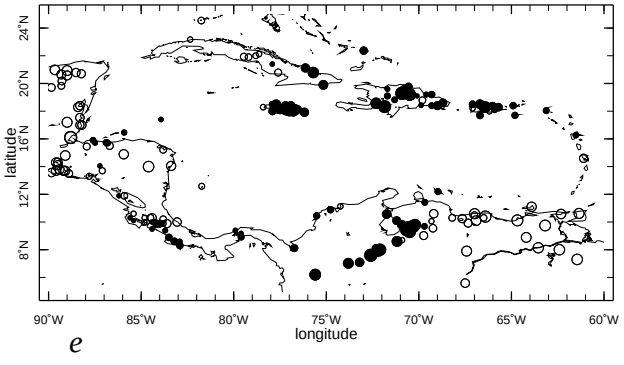
24°N
20°N
16°N
12°N
8°N
latitude
90°W
85°W
80°W
75°W
70°W
65°W
60°W
longitude

e

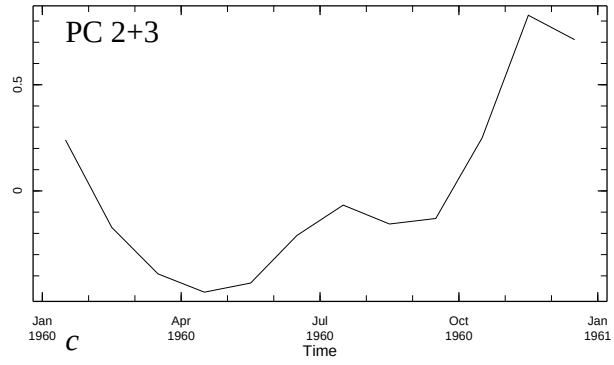
PC 2+3
0.5
0
Jan 1960
Apr 1960
Jul 1960
Oct 1960
Jan 1961
Time

c

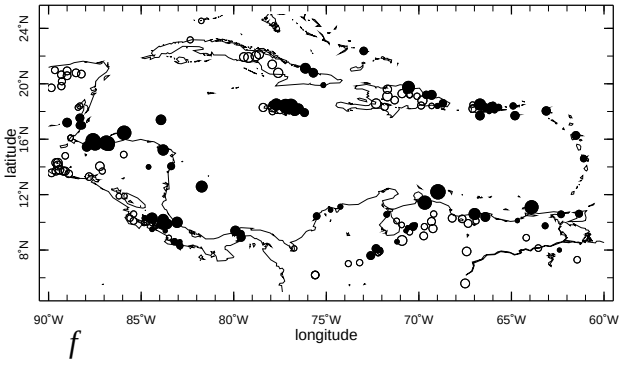
24°N
20°N
16°N
12°N
8°N
latitude
90°W
85°W
80°W
75°W
70°W
65°W
60°W
longitude

f

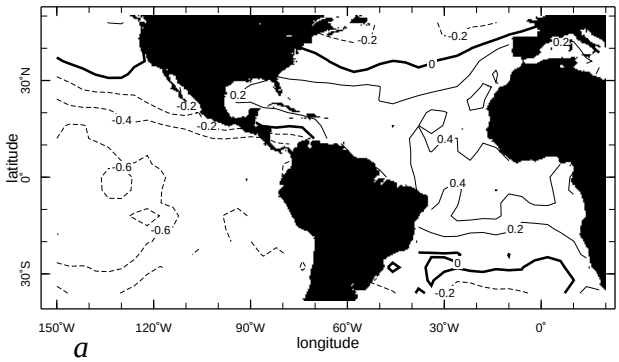
30°N
0°
30°S
latitude
150°W
120°W
90°W
60°W
30°W
0°
longitude
-0.2
0
0.2
-0.4
0.4
-0.6
0.6

a

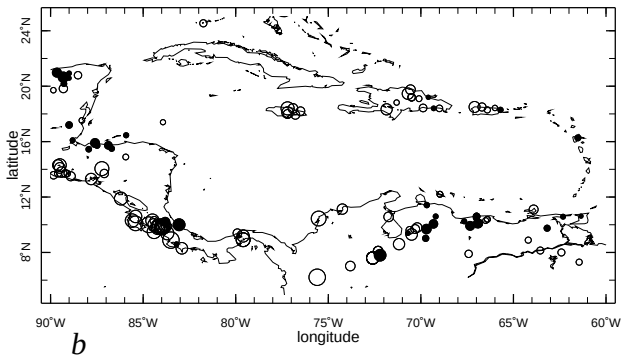
24°N
20°N
16°N
12°N
8°N
latitude
90°W
85°W
80°W
75°W
70°W
65°W
60°W
longitude

b

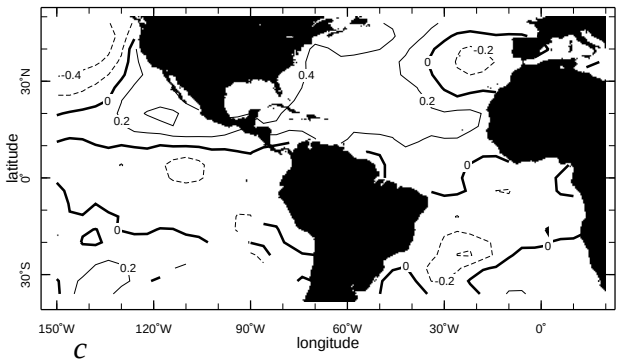
30°N
0°
30°S
latitude
150°W
120°W
90°W
60°W
30°W
0°
longitude
-0.4
0.4
0
0.2
-0.2

c

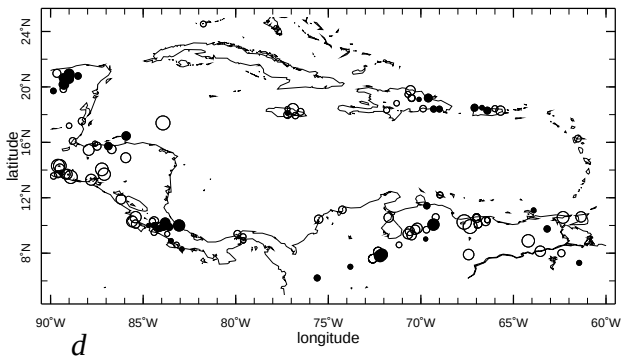
24°N
20°N
16°N
12°N
8°N
latitude
90°W
85°W
80°W
75°W
70°W
65°W
60°W
longitude

d

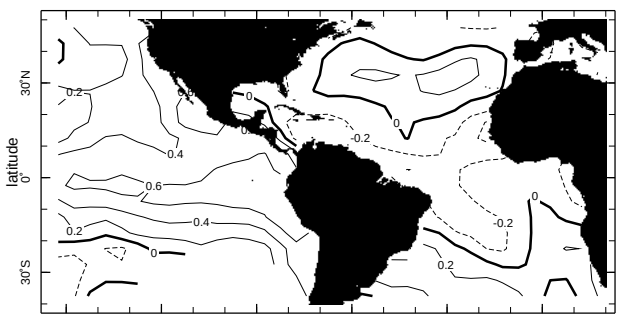
30°N
0°
30°S
latitude
150°W
120°W
90°W
60°W
30°W
0°
longitude

a

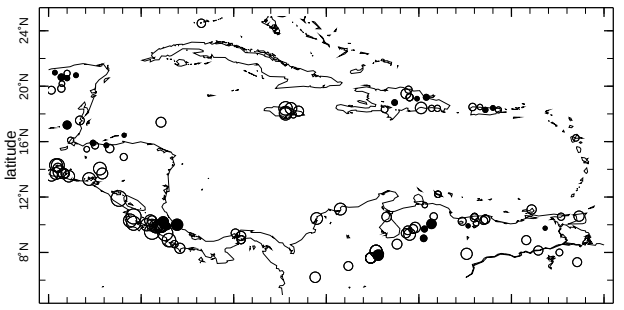
24°N
20°N
16°N
12°N
8°N
latitude
90°W
85°W
80°W
75°W
70°W
65°W
60°W
longitude

b

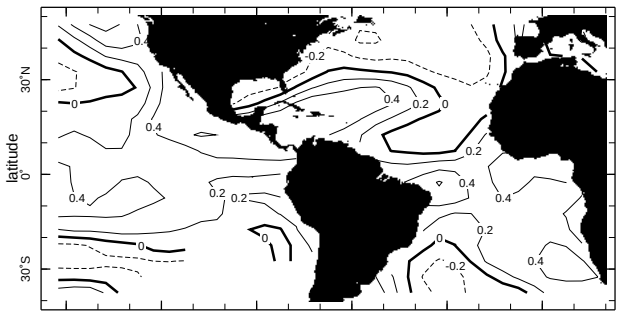
30°N
0°
30°S
latitude
150°W
120°W
90°W
60°W
30°W
0°
longitude

c

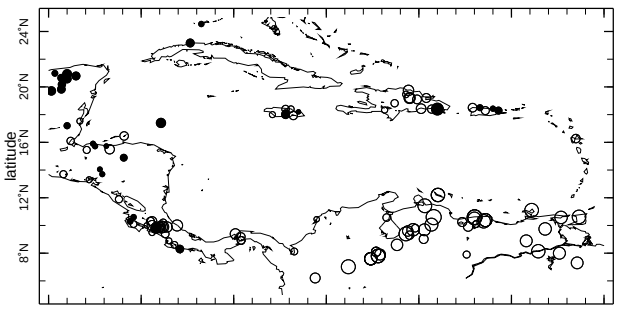
24°N
20°N
16°N
12°N
8°N
latitude
90°W
85°W
80°W
75°W
70°W
65°W
60°W
longitude

d

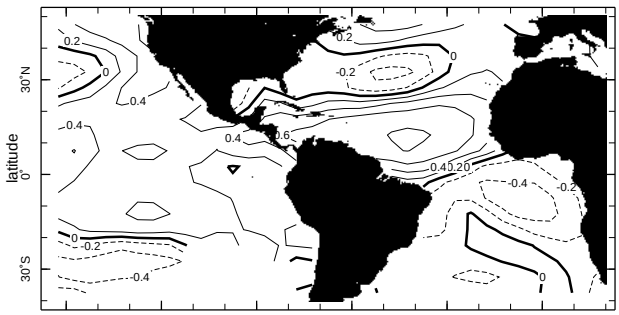
30°N
0°
30°S
latitude
150°W
120°W
90°W
60°W
30°W
0°
longitude

e

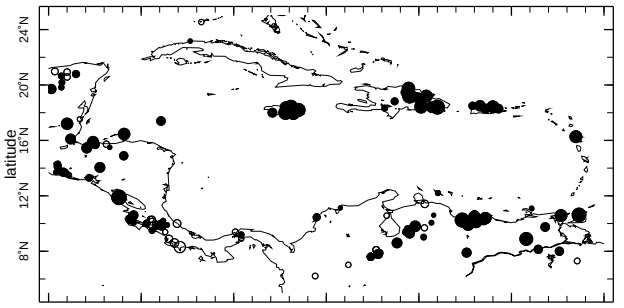
24°N
20°N
16°N
12°N
8°N
latitude
90°W
85°W
80°W
75°W
70°W
65°W
60°W
longitude

f

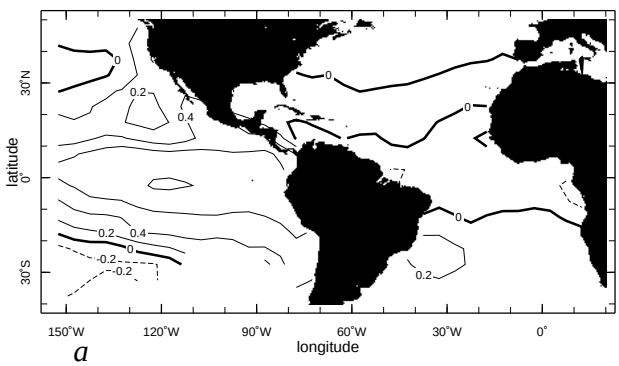
30°N
0°
30°S
latitude
150°W
120°W
90°W
60°W
30°W
0°
longitude

a

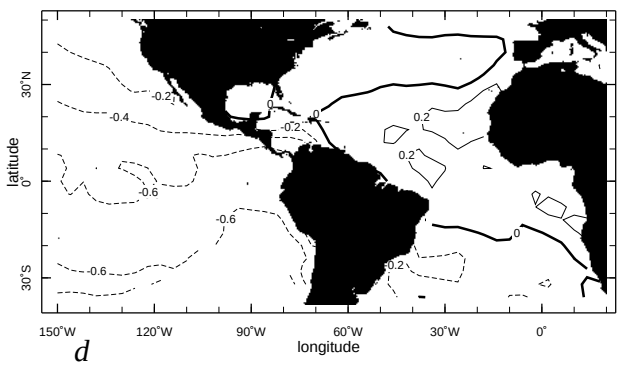
30°N
0°
30°S
latitude
150°W
120°W
90°W
60°W
30°W
0°
longitude

d

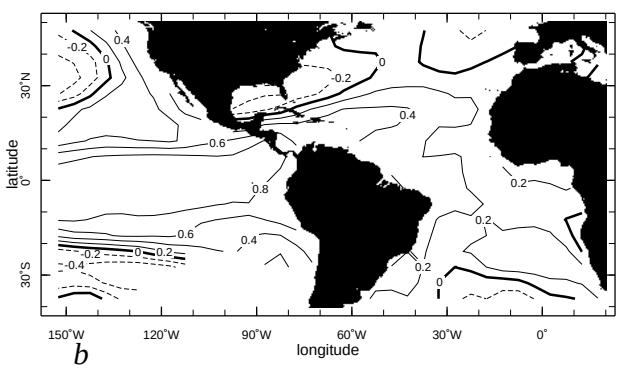
30°N
0°
30°S
latitude
150°W
120°W
90°W
60°W
30°W
0°
longitude

b

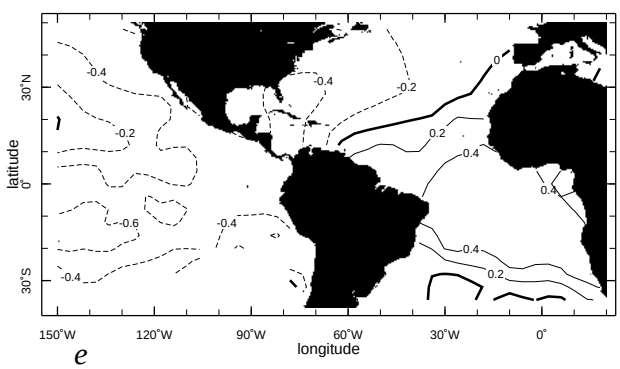
30°N
0°
30°S
latitude
150°W
120°W
90°W
60°W
30°W
0°
longitude

e

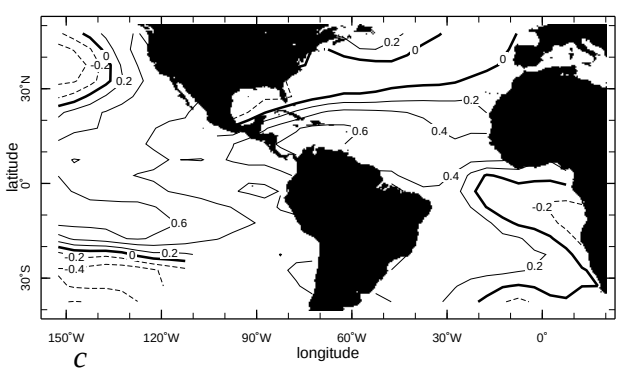
30°N
0°
30°S
latitude
150°W
120°W
90°W
60°W
30°W
0°
longitude

c

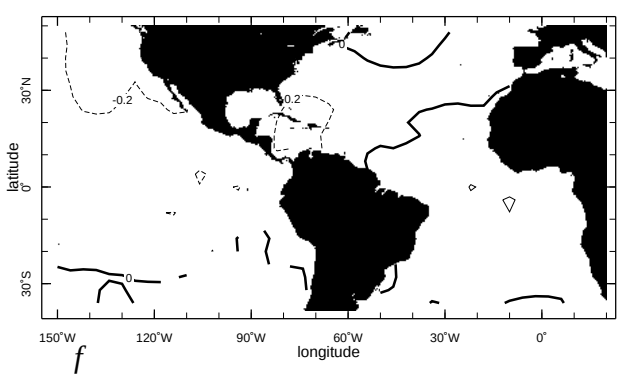
30°N
0°
30°S
latitude
150°W
120°W
90°W
60°W
30°W
0°
longitude

f

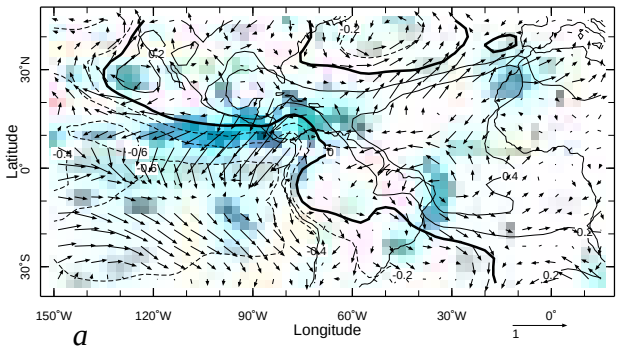

a

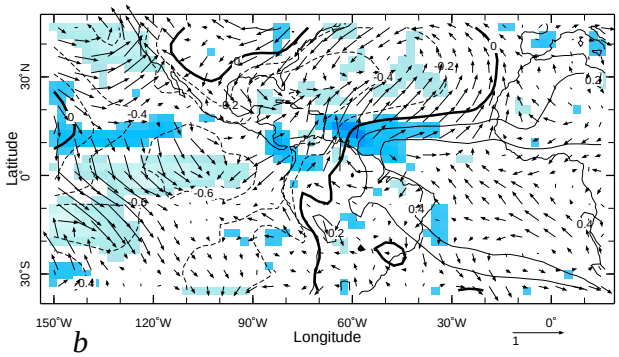

b

1000 mb

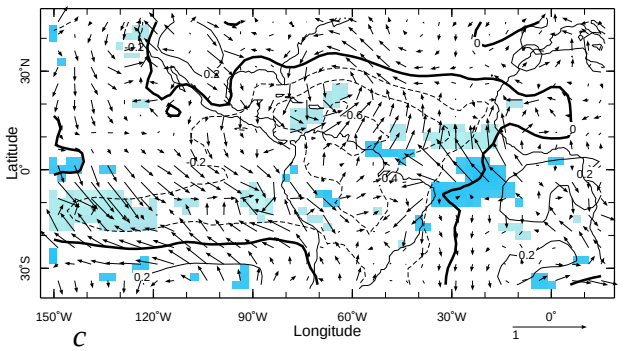

c

1000 mb

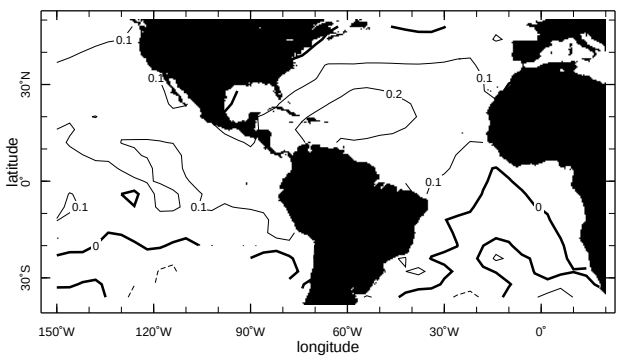
30°N
0°
30°S
latitude
150°W
120°W
90°W
60°W
30°W
0°
longitude

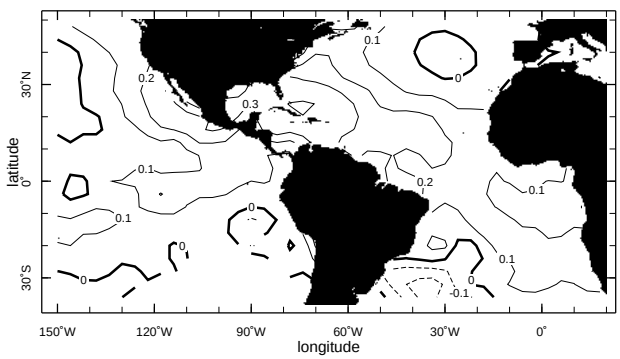
30°N
0°
30°S
latitude
150°W
120°W
90°W
60°W
30°W
0°
longitude

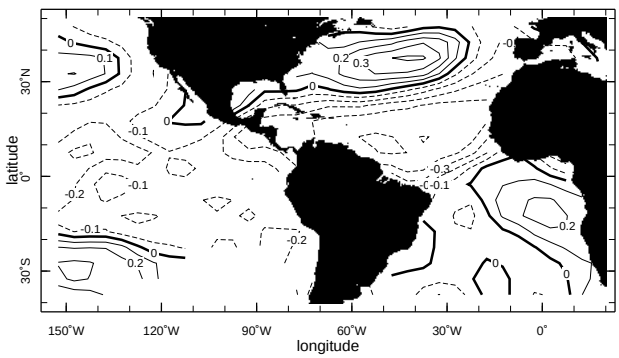
30°N
0°
30°S
latitude
150°W
120°W
90°W
60°W
30°W
0°
longitude

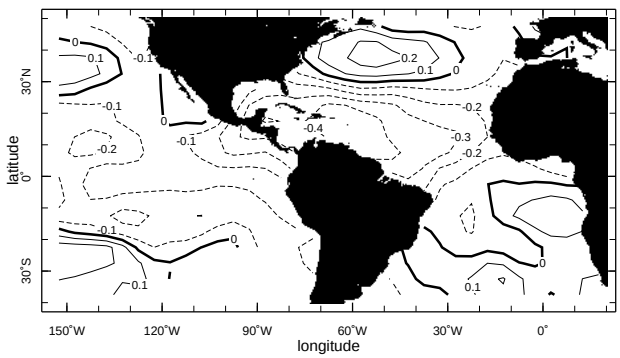
30°N
0°
30°S
latitude
150°W
120°W
90°W
60°W
30°W
0°
longitude

Figure Captions

Figure 1. Principal Component Analysis of the annual cycle. Left column, time coefficients: (top) PC 1, (middle) PC2 minus PC3, and (bottom) is PC2 plus PC3; right column: the corresponding spatial patterns. Full black circles are positive spatial loadings onto the corresponding (linear combination of) PC, open circles are negative spatial loadings.

Figure 2. Canonical correlation analysis of SLP and rainfall: *Heterogeneous* correlation maps. Upper panels: the July-August inter-basin SLP pattern (left) and corresponding rainfall pattern (right). Positive contours are solid, negative contours are dashed, contour is 0.2; positive rainfall anomalies are in full black circles, negative anomalies are in open circles. Lower panels: the July-August Atlantic pattern.

Figure 3. Canonical correlation analysis of SST and rainfall: *Heterogeneous* correlation maps. Upper panels: July-August inter-basin mode. Middle panels: January-February inter-basin mode. Lower panels: May-June Atlantic mode.

Figure 4. Correlation maps of the NINO3 index, averaged over Dec(0)-Jan(+1), with SST (left column) in: (top) Jul-Aug (0), (middle) Jan-Feb (+1), and (bottom) May-Jun (+1), and with SLP (right column) in: (top) Jul-Aug (0), (middle) Jan-Feb (+1) and (bottom) May-Jun (+1). Contour is 0.2.

Figure 5. Correlation maps of the NINO3 index, averaged over Dec(0)-Jan(+1), with NCEP-NCAR Reanalysis SLP (contours), divergence (shading) and winds (arrows) in: (top) Jul-Aug (0), (middle) Jan-Feb (+1), and (bottom) May-Jun (+1). Contour is 0.2; negative values are dashed, positive values are solid, and the thick black line is the zero correlation line. Shading is light for negative correlation values, dark for positive ones; absolute values less than 0.3 are not shaded.

Figure 6. Correlation maps of the North Atlantic High index, averaged over December-March, with SLP and SST fields during the following May-Jun and Jul-Aug. SLP and North Atlantic High index correlations are displayed in the left column; SST and North Atlantic High index correlations are displayed in the right column. Contour is 0.1.

	PC	*janfeb*	*marapr*	*mayjun*	*julaug*	*sepoct*	*novdec*
SLP	1	32	25	32	27	29	31
	2	20	19	16	22	23	17
	3	14	10	12	9	9	10
SLP	*tot*	66	54	60	58	61	58
SST	1	26	26	22	19	23	25
	2	12	14	12	12	12	12
	3	10	10	10	11	10	10
SST	*tot*	48	50	44	42	45	47
prcp	1	22	19	19	18	18	21
	2	10	12	13	9	8	12
prcp	*tot*	32	31	32	27	26	33

	r(NINO3,PC1)	r(tAtl,PC2)	r(NAtl Hi,PC3)
janfeb	(0.37) (+1)	0.74	0.58
marapr	0.59 (+1)	0.86	0.72
mayjun	0.73 (0)	0.71	0.89
julaug	0.82 (0)	0.98	0.78
sepoct	0.77 (0)	0.91	0.46
novdec	0.78 (0)	0.71	0.49

	r(NINO3,PC1)	r(Atl SST Dipole,PC2)	r(Atl SST Dipole,PC3)
janfeb	0.86 (+1)	0.85	(0.30)
marapr	0.72 (+1)	0.84	(0.12)
mayjun	0.55 (+1)	0.55	0.55
julaug	0.73 (0)	0.64	0.65
sepoct	0.89 (0)	0.72	0.51
novdec	0.89 (0)	0.47	0.79

	SLP interbasin mode	*SLP NAtl mode*	*SST ENSO mode*	*SST NAtl mode*
janfeb	0.48	0.52	0.57*	0.22
marapr	0.38	0.15	0.34	0.23
mayjun	0.29	0.07	0.67*	0.11
julaug	0.70*	0.52*	0.68*	0.69
sepoct	0.79	0.27	0.60	0.44
novdec	0.58	0.49	0.53	0.19

	janfeb	*marapr*	*mayjun*	*julaug*	*sepoct*	*novdec*
SLP interbasin mode	12	12	15	13	18	21
SLP NAtl mode	17	20	16	11	8	12
SST ENSO mode	16	12	18	19	18	21
SST NAtl mode	13	20	14	9	8	12

Table Captions

Table 1. The percent of total variance explained in each two-month interval by the first three principal components of SLP and SST, and by the first two principal components of rainfall (prcp).

Table 2. Correlations of the PCs of slp with relevant climatic indices. *Column 1*: PC1 and NINO3, with NINO3 averaged over Dec(0)-Jan(+1). *Column 2*: PC2 and tropical Atlantic slp, averaged between 15°S and 15°N, and 60°W and 30°W. *Column 3*: PC3 and the North Atlantic High Index. Correlations in columns 2 and 3 are simultaneous.

Table 3. Correlations of the PCs of SST with relevant climatic indices. *Column 1*: PC1 and NINO3, averaged during December (0)-January (+1). '(0)' and '(+1)' denote bimonthly periods belonging to year (0) and (+1) of an event, respectively. *Columns 2* and *3*: PCs 2 and 3 and the Atlantic SST Dipole Index (see text for a definition). Correlations in columns 2 and 3 are simultaneous.

Table 4. Correlations between the CCA time series for the slp or SST mode and the corresponding rainfall mode. Modes denoted by an asterisk are shown in figures 2 and 3.

Table 5. The percent of total variance of rainfall explained in each two-month interval by the modes of CCA of SLP/SST and rainfall.